

Second Order Models and Traffic Data from Mobile Sensors

Benedetto Piccoli^{a*} Ke Han^{b†} Terry L. Friesz^{c‡} Tao Yao^{c§}

^a*Department of Mathematics, Rutgers University, NJ 08102, USA*

^b*Department of Mathematics, Pennsylvania State University, PA 16802, USA*

^c*Department of Industrial and Manufacturing Engineering,
Pennsylvania State University, PA 16802, USA*

Abstract

Mobile sensing enabled by on-board GPS or smart phones has become the primary source of traffic data. For sufficient coverage of the traffic stream, it is important to maintain a reasonable penetration rate of probe vehicles. From the standpoint of estimating higher-order traffic quantities such as acceleration/deceleration, emission rate and fuel consumption rate, it is desirable to examine the effectiveness of sampling frequency of current sensing technology in capturing higher-order variations inherent in traffic stream. Of the two concerns raised above, the latter is rarely studied in the literature.

In this paper, we study the two characteristics of mobile sensing: penetration rate and sampling frequency, and their impacts on the quality of traffic estimation. A computational method is presented that integrates vehicle trajectory data into a second-order hydrodynamic model known as the *phase transition model* (Colombo, 2002a). We utilize the *Next Generation SIMulation* (NGSIM, 2006) dataset containing high time-resolution vehicle trajectories. It is demonstrate through extensive numerical study that while first-order traffic quantities can be accurately estimated using prevailling sampling frequency at a reasonably low penetration rate, higher-order traffic quantities tend to be misinterpreted due to insufficient sampling frequency of current mobile devices. We propose, for estimating emission and fuel consumption rates, a correction factor approach which is proven to yield improved accuracy via statistical validation.

1 Introduction

1.1 Mobile sensing

In the era of mobile internet, mobile sensors such as *global positioning system* (GPS) and smart phones have become the primary means of collecting traffic-related information (Herrera et al., 2010). Attractive features of GPS-based mobile sensing includes potentially complete spatial and temporal coverage of the traffic network and high positioning accuracy. Traffic data on first-order quantities, including velocity, density, and travel time, are often processed in connection with first-order traffic flow models such as the Lighthill-Whitham-Richards model (Lighthill and Whitham, 1955; Richards, 1956) or its discrete versions such as the *cell transmission model* (Daganzo, 1994, 1995), with an incomplete list of references including

*e-mail: piccoli@camden.rutgers.edu

†e-mail: kxh323@psu.edu;

‡e-mail: tfriesz@psu.edu;

§e-mail: tyyl1@enr.psu.edu;

Claudel and Bayen (2010a,b); Wang and Papageorgiou (2005); Work et al. (2010); Yuan et al. (2011). Another important class of data, namely, higher-order traffic quantities including acceleration/deceleration, emission and fuel consumption rates, are not immediately available through traditional mobile sensing technologies and are insufficiently captured by first-order models.

In addition, existing study on mobile sensing is primarily concerned with the penetration rate of probe vehicles (Demers et al., 2006; Kwon et al., 2007; Yim and Cayford, 2001); little attention is raised on the impact of sampling frequency on the quality of estimation, especially regarding higher-order traffic quantities. Typical mobile sensors such as GPS report the location of a probe vehicle every 3 – 4 seconds, thus derived information on velocity and acceleration etc. is averaged in the same time period. However, there exist higher-order variations inherent in traffic stream that take place on a much smaller time scale, especially when the traffic is congested and unstable. Many of those higher-order variations are unaccounted for by existent sensing paradigms.

This paper addresses the issue of estimating both first-order and higher-order traffic quantities mentioned above, by employing a second-order traffic flow model known as the *phase transition model* (PTM) (Colombo, 2002a) as well as its variances. The dataset under consideration is provided by the *Next Generation SIMulation* (NGSIM) ¹ which contains high-resolution vehicle trajectories on a segment of I-80, California. The NGSIM data records the location of each passing vehicle every 0.1 second. Such high precision in trajectories provides unique information, especially on higher-order variations, of traffic stream that is unavailable through traditional mobile devices or fixed sensors. We propose several computational schemes for reconstructing Eulerian and Lagrangian traffic quantities, using vehicle trajectory data as input. We will demonstrate how the quality of estimation deteriorates with less frequent sampling of vehicle locations and with lower probe penetration rate. In particular, we will evaluate the performance of existent sensing devices (GPS) in reconstructing first- and higher-order quantities.

The main findings confirm our earlier observation that the estimation of higher-order traffic quantities deteriorates by a discernible amount when the sampling frequency decreases, while the estimation of first-order quantities remain relatively accurate in the same situation. Similar experiment is performed using different probe penetration rates. The numerical results demonstrate robustness of the proposed estimation method in recovering first-order traffic quantities under low sampling frequency and penetration rate. Nevertheless, higher-order quantities such as tailpipe emission rate and fuel consumption rate tend to be underestimated due to the negligence of higher-order variations in acceleration/deceleration that is caused by the prevailing three-second sampling period. We propose a correction factor approach which is proven to yield improved accuracy in estimating emission and fuel consumption rates via statistical validation.

This paper takes the unique advantage of 100 % coverage of traffic stream at a high time-resolution provided by the NGSIM dataset. Insights regarding GPS sensing drawn from our numerical test is wholly original and serves the practical purpose of developing traffic monitoring infrastructure under which more accurate emission and fuel consumption profiles can be reconstructed.

¹<http://ngsim-community.org/>

1.2 The phase transition model

The hyperbolic *phase transition model* (PTM) for traffic flow is first introduced by Colombo (2002a) and Colombo (2002b), and studied subsequently by Colombo and Corli (2002); Colombo et al. (2007) and Blandin et al. (2012). The PTM belongs to a class of traffic models recognized as *second-order*, as it captures second-order variations in traffic in addition to average velocity and density. Other second-order models include the Payne-Whitham model proposed independently by Payne (1971, 1979) and Whitham (1974), and the Aw-Rascle-Zhang model developed by Aw and Rascle (2000) and Zhang (2002). The phase transition model is motivated by the empirical observation that when the vehicle density exceeds certain value, the density-flow pairs are scattered in a two-dimensional region, instead of forming certain one-to-one relationship as asserted by the classical Lighthill-Whitham-Richards (LWR) model (Lighthill and Whitham, 1955; Richards, 1956).

The PTM consists of two phases: the uncongested phase and the congested phase. In the uncongested phase, the dynamic is governed by the LWR model

$$\begin{cases} \rho_t + [\rho \cdot v]_x = 0 \\ v = v(\rho) \end{cases} \quad (1.1)$$

where velocity is expressed as a function of only density. The congested phase, on the other hand, is governed by the following system of conservation laws:

$$\begin{cases} \rho_t + [\rho \cdot v]_x = 0 \\ q_t + [(q - q^*) \cdot v]_x = 0 \\ v = v(\rho, q) \end{cases} \quad (1.2)$$

where the velocity $v(\rho, q)$, in contrast to (1.1), depends not only on local density ρ , but also on q which is identified as the perturbation or deviation. q^* is a given parameter. One choice for $v(\rho, q)$ is

$$v(\rho, q) = \left(1 - \frac{\rho}{\rho_{jam}}\right) \cdot \frac{q}{\rho} \quad (1.3)$$

where ρ_{jam} denotes the jam density. Another choice is

$$v(\rho, q) = A(\rho_{jam} - \rho) + B(q - q^*)(\rho_{jam} - \rho) \quad (1.4)$$

for some given parameters A and B .

One has a lot of freedom in choosing the second-order model for the congested phase. For instance, Goatin (2006) proposes a phase-transition model which employs the Aw-Rascle-Zhang equations (Aw and Rascle, 2000; Zhang, 2002) for the congested phase. Furthermore, we can consider the modified PTM by taking into account the reaction time of drivers. More specifically, following Siebel and Mauser (2006a), we write

$$q_t + [(q - q^*) \cdot v]_x = \frac{q - q^*}{T - \tau} \quad (1.5)$$

as the equation for the congested phase. The right hand side is called the Siebel-Mauser source term. Here τ is a reaction time. Typically τ (in second) varies within $[0.5, 1]$. One should compute T as the time at which the velocity is essentially at equilibrium. In Siebel and Mauser (2006a), T is chosen to be 2/3 second. Finally $T - \tau$ is modeled as a factor which can be positive (for very small or very high densities) or negative (for intermediate densities). One has to notice that a negative factor gives rise to stable traffic, while a positive ones produces instabilities.

1.3 Data description

Initiated by the United States Department of Transportation (US DOT) Federal Highway Administration (FHWA) in the early 2000's, the Next Generation SIMulation (NGSIM, 2006) program collected high-quality primary traffic and trajectory data intended to support the research and testing of the traffic models and open behavioral algorithms.

We take the I-80 data set collected and processed on a segment of Interstate 80 located in Emeryville, California on Apr. 13, 2005. A total of 45 minutes of data are available, segmented into three 15 minute periods. The data set contains vehicle trajectory, instantaneous velocity and acceleration recorded at a high precision of every 0.1 second. By neglecting sensing and processing error, we treat the raw data set as the ground-truth traffic state.

Upon acquisition of high quality vehicle trajectory data, we are interested in the following research issues that have a substantial impact on the modeling and computational paradigms of vehicular traffic.

- How does the estimation of first order and second order traffic quantities deteriorate with less frequent sampling of vehicle locations. In particular, is the prevailing sampling frequency of on-board devices such as smart phones and GPS sufficient to reconstruct various types of traffic data?
- What effect the penetration rate of probe vehicles has on the quality of traffic quantities mentioned above?
- The performance of second order traffic flow models with various modeling assumptions in estimating traffic quantities.
- Are there practical ways to reconstruct emission and fuel consumption rates accurately with vehicle trajectory data obtained from GPS at a low penetration rate?

All these questions will be addressed in subsequent discussion.

1.4 Organization

The rest of this paper is organized as follows. Section 2 describes numerical techniques for transforming vehicle trajectory data into various Eulerian and Lagrangian quantities to be integrated with the traffic model. This is followed by three different ways of fitting the traffic data to the phase transition model under various assumptions, which is presented in Section 3. In Section 4, the phase transition model is calibrated using the NGSIM field data. It also contains a comprehensive discussion of the dataset and its characteristics. Section 5 assesses the estimation quality of first- and second-order quantities along vehicle trajectories, when the sampling frequencies change. In Section 6, we reconstruct Eulerian-based quantities, that is, cell-based densities, emission rate and fuel consumption rate. The latter two both are higher-order quantities and are not sufficiently captured by GPS data. We propose a correction factor which yields accurate estimation under statistical validation.

2 Traffic Data Measurements

Using onboard devices such as GPS or smart phone, it is possible to measure the position of a car every δt seconds. Here δt is related to the device's characteristics such as desired precision and transmission capacity. Let us denote $x(t)$ the position and $v(t)$ the velocity

at time t . Assume we measure the position at three consecutive shots t_1, t_2 and t_3 with $t_2 - t_1 = t_3 - t_2 = \delta t$ (say around 3 seconds for GPS). From these measurements we can deduce the approximate velocities in the intervals $[t_1, t_2]$ and $[t_2, t_3]$ as:

$$v_{1,2} = \frac{x(t_2) - x(t_1)}{\delta t}, \quad v_{2,3} = \frac{x(t_3) - x(t_2)}{\delta t}. \quad (2.6)$$

The velocity at time t_2 is approximated as

$$v(t_2) \sim \frac{v_{1,2} + v_{2,3}}{2} = \frac{x(t_3) - x(t_1)}{2\delta t} \quad (2.7)$$

One also gets

$$\frac{D}{Dt}v(t_2) \sim \frac{v_{2,3} - v_{1,2}}{\delta t} = \frac{x(t_3) - 2x(t_2) + x(t_1)}{\delta t^2} \quad (2.8)$$

where $D/Dt = d/dt + v \cdot d/dx$ denotes the material derivative in eulerian coordinates corresponding to the acceleration of the car in Lagrangian ones.

Another important quantity to estimate is the spatial variation of velocity in Eulerian coordinates. For shorter notation, we denote $x_i \doteq x(t_i)$. Assuming a mild variation in time of the eulerian velocity $v(t, x)$, we write:

$$v\left(t_2, \frac{x_2 + x_1}{2}\right) \sim v_{1,2}, \quad v\left(t_2, \frac{x_3 + x_2}{2}\right) \sim v_{2,3},$$

from which we get, setting $\delta x = \frac{x_3 + x_2}{2} - \frac{x_2 + x_1}{2}$:

$$\frac{\partial}{\partial x}v\left(t_2, \frac{\frac{x_3 + x_2}{2} + \frac{x_2 + x_1}{2}}{2}\right) \sim \frac{v_{2,3} - v_{1,2}}{\delta x}$$

in other words:

$$\frac{\partial}{\partial x}v\left(t_2, \frac{x_3 + 2x_2 + x_1}{4}\right) \sim \frac{v_{2,3} - v_{1,2}}{\frac{x_3 - x_1}{2}} = \frac{2}{\delta t} \frac{x_3 - 2x_2 + x_1}{x_3 - x_1} \quad (2.9)$$

Clearly such approximation is acceptable as long as the variation between $v_{1,2}$ and $v_{2,3}$ is not too large.

3 Traffic Quantities and Model Fitting using Mobile Data

Depending on the choice of the model and the level of approximation we can use the obtained traffic data in many ways to fit an evolutive model (with Kalman filter or other methods). Let us describe in this section some choices which can be used depending on traffic data type, level of accuracy and computational constraints.

3.1 Phase transition model

We depart from the basic phase transition model introduced in Section 1.2. First note that one should determine two critical velocities V_f and V_c , and use either the LWR model (i.e. the model corresponding to the uncongested phase) if $v \geq V_f$; or the second-order model if $v < V_c$. In this paper, we will primarily focus on the second case, since this is where higher-order phenomena take place.

3.1.1 Phase transition model with source and strongly stable traffic

We consider the phase transition model (Colombo, 2002a,b) with velocity in the congested phase given by

$$v(\rho, q) = A(\rho_{jam} - \rho) + B(q - q^*)(\rho_{jam} - \rho) \quad (3.10)$$

In addition, we add a Siebel-Mauser type source term. Thus the equation for the congested phase is given by:

$$q_t + [v(q - q^*)]_x = \frac{q - q^*}{T - \tau} \quad (3.11)$$

Assume that the traffic is strongly stable, that is, during the data measurement we may assume $\rho_t, \rho_x, q_x \approx 0$ with only q_t being non-vanishing. Following Siebel and Mauser (2006a), we let $T \sim 2/3$ second and $\tau \sim 1$ second. Therefore $T - \tau \sim -1/3$ second. By the strongly stability assumption, (3.11) reduces to

$$q_t = \frac{q - q^*}{T - \tau} \quad (3.12)$$

Then we can derive

$$\frac{D}{Dt}v = \partial_t v(\rho(t, x), q(t, x)) + v \cdot \partial_x v(\rho(t, x), q(t, x)) \quad (3.13)$$

$$= v_\rho \cdot \rho_t + v_q \cdot q_t + v \cdot (v_\rho \cdot \rho_x + v_q \cdot q_x) \quad (3.14)$$

$$= v_q \cdot q_t \quad (3.15)$$

$$= B(\rho_{jam} - \rho) \cdot \frac{q - q^*}{T - \tau} \quad (3.16)$$

$$= -3B(\rho_{jam} - \rho)(q - q^*) = -3(v - A(\rho_{jam} - \rho)) \quad (3.17)$$

From (3.12), we get

$$(q - q^*)_t = q_t = \frac{q - q^*}{T - \tau} = -3(q - q^*) \quad (3.18)$$

Taking into account only the measurements of v and Dv/Dt , we deduce from (3.17) that

$$(\rho_{jam} - \rho) = \frac{1}{A} \left(v + \frac{1}{3} \frac{Dv}{Dt} \right) \quad (3.19)$$

$$(q - q^*) = -\frac{1}{3} \frac{A}{B} \frac{\frac{Dv}{Dt}}{v + \frac{1}{3} \frac{Dv}{Dt}} \quad (3.20)$$

Following the discussion in Section 2, the quantity v is computed according to (2.7), while the quantity Dv/Dt is computed according to (2.8).

3.1.2 Phase transition model with source and less strongly stable traffic

In this case, we rely on the less strongly stable assumption on traffic. In other words, we no longer assume that ρ_x vanishes, while still neglecting ρ_t and q_x . Then equation (3.11) becomes

$$q_t + v_x(q - q^*) = \frac{q - q^*}{T - \tau} \quad (3.21)$$

We can now write

$$\frac{Dv}{Dt} = v_t + vv_x \sim v_q q_t + vv_x = v_q \left(\frac{q - q^*}{T - \tau} - (q - q^*)v_x \right) + vv_x \quad (3.22)$$

By introducing the variables $\hat{\rho} \doteq \rho_{jam} - \rho$, $\hat{q} \doteq q - q^*$, we obtain

$$v = A(\rho_{jam} - \rho) + B(q - q^*)(\rho_{jam} - \rho) = \hat{\rho}(A + B\hat{q}) \quad (3.23)$$

and deduce from (3.23) that

$$\frac{Dv}{Dt} - vv_x = v_q \left(\frac{\hat{q}}{T - \tau} - \hat{q}v_x \right) = B\hat{\rho} \left(\frac{\hat{q}}{T - \tau} - \hat{q}v_x \right) \quad (3.24)$$

From (3.23), (3.24) we immediately get the expressions for $\hat{\rho}$ and \hat{q} in terms of v , v_x and $\frac{Dv}{Dt}$.

$$\hat{\rho} = v \frac{v - (T - \tau) \frac{Dv}{Dt}}{A(v - (T - \tau)vv_x)} \quad (3.25)$$

$$\hat{q} = \frac{A}{B} \frac{(T - \tau) \left(\frac{Dv}{Dt} - vv_x \right)}{v - (T - \tau) \frac{Dv}{Dt}} \quad (3.26)$$

The quantities $\frac{Dv}{Dt}$, v_x are given by (2.8) and (2.9) respectively. Notice that if we approximate v with (2.6), then

$$\begin{aligned} \frac{Dv}{Dt} - vv_x &\sim \frac{x(t_{i+1}) - 2x(t_i) + x(t_{i-1}))}{\delta t^2} \\ &\quad - \frac{x(t_{i+1}) - x(t_{i-1}))}{2\delta t} \cdot \frac{2}{\delta t} \cdot \frac{x(t_{i+1}) - 2x(t_i) + x(t_{i-1}))}{x(t_{i+1}) - x(t_{i-1}))} \equiv 0. \end{aligned} \quad (3.27)$$

Therefore to avoid such a trivial case, one should instead approximate v by either

$$v(t_2) \sim v_{1,2} = \frac{x(t_2) - x(t_1)}{\delta t}, \quad \text{or} \quad v(t_2) \sim v_{2,3} = \frac{x(t_3) - x(t_2)}{\delta t}$$

3.1.3 Phase transition model without source term

In this case, we consider the PTM without the Siebel-Mauser type source term:

$$\begin{cases} \rho_t + (\rho \cdot v)_x = 0 \\ q_t + ((q - q^*) \cdot v)_x = 0 \\ v(\rho, q) = A(\rho_{jam} - \rho) + B(q - q^*)(\rho_{jam} - \rho) \end{cases} \quad (3.28)$$

We start with the identity

$$\frac{Dv}{Dt} = v_t + v \cdot v_x = v_\rho \rho_t + v_q q_t + v(v_\rho \rho_x + v_q q_x).$$

Using (3.28), we deduce

$$\begin{aligned} \frac{Dv}{Dt} &= v_\rho(-\rho_x v - \rho v_x) + v_q(-q_x v - (q - q^*)v_x) + v(v_\rho \rho_x + v_q q_x) \\ &= -v_x(v_\rho \rho + v_q(q - q^*)). \end{aligned}$$

If we consider the measurements of v , Dv/Dt and also v_x as indicated in Section 2 then we can consider the two relations:

$$v = A(\rho_{jam} - \rho) + B(q - q^*)(\rho_{jam} - \rho) \quad (3.29)$$

$$\frac{Dv}{Dt} = v_x(A\rho + B(q - q^*)(2\rho - \rho_{jam})). \quad (3.30)$$

Recall the variables $\hat{\rho} = \rho_{jam} - \rho$ and $\hat{q} = q - q^*$. Combining (3.29) and (3.30) and solving for ρ we get:

$$\rho = \frac{1}{B\hat{q}} \left(v + \frac{1}{v_x} \frac{Dv}{Dt} - A\rho_{jam} \right) \quad (3.31)$$

So \hat{q} and $v + \frac{1}{v_x} \frac{Dv}{Dt} - A\rho_{jam}$ always have the same sign. Substituting (3.31) into (3.29), we get

$$B^2\rho_{jam}\hat{q}^2 + B \left(2A\rho_{jam} - \frac{1}{v_x} \frac{Dv}{Dt} - 2v \right) \hat{q} - A \left(v + \frac{1}{v_x} \frac{Dv}{Dt} - A\rho_{jam} \right) = 0 \quad (3.32)$$

The discriminant of the above quadratic equation in the variable \hat{q} is

$$\begin{aligned} \Delta &= 4B^2 \left(v + \frac{1}{2} \frac{1}{v_x} \frac{Dv}{Dt} - A\rho_{jam} \right)^2 + 4AB^2\rho_{jam} \left(v + \frac{1}{v_x} \frac{Dv}{Dt} - A\rho_{jam} \right) \\ &= 4B^2 \left(\left(v + \frac{1}{2} \frac{1}{v_x} \frac{Dv}{Dt} \right)^2 - A\rho_{jam}v \right) \end{aligned} \quad (3.33)$$

In order for any meaningful real root of (3.32) to exist, a necessary condition is that Δ is nonnegative, leading to

$$\left| v + \frac{1}{2} \frac{1}{v_x} \frac{Dv}{Dt} \right| \geq \sqrt{A\rho_{jam}v} \quad (3.34)$$

In the case where the strict inequality of (3.34) holds, two distinct roots \hat{q}_1 and \hat{q}_2 exist. We distinguish between two cases:

- If

$$v + \frac{1}{v_x} \frac{Dv}{Dt} - A\rho_{jam} > 0 \quad (3.35)$$

Then $\hat{q}_1\hat{q}_2 < 0$. Equation (3.32) has one positive root and one negative root. By (3.31), one should choose the positive root since ρ must be non-negative.

- If

$$v + \frac{1}{v_x} \frac{Dv}{Dt} - A\rho_{jam} \leq 0 \quad (3.36)$$

Then $\hat{q}_1\hat{q}_2 \geq 0$. Equation (3.32) has two roots with the same sign². In view of (3.31) and (3.36), to ensure that ρ is nonnegative, both \hat{q}_1 and \hat{q}_2 should be nonpositive and at least one root is negative. This in turn requires that

$$2A\rho_{jam} - \frac{1}{v_x} \frac{Dv}{Dt} - 2v > 0 \quad (3.37)$$

In view of (3.36), a sufficient condition for (3.37) to hold is $\frac{1}{v_x} \frac{Dv}{Dt} > 0$. We will have more to say about these logical conditions when we introduce discrete-time approximations later in Section 5.

²zero is considered to have both positive sign and negative sign.

3.2 Estimation of emission and fuel consumption

We consider an emission and fuel consumption model that considers the modal operation of a vehicle, that is, emission/fuel consumption is directly related to vehicle operating modes such as idle, steady-state cruise, acceleration and deceleration. This model relies on high time-resolution vehicle trajectory data which is naturally available thanks to the NGSIM dataset. According to the power demand-based emission/fuel consumption model proposed by Post et al. (1984), the overall instantaneous total power demand Z for a vehicle with mass m (in kg) is given by

$$Z = (0.04v + 0.5 \times 10^{-3}v^2 + 10.8 \times 10^{-6}v^3) + \frac{m}{1000} \frac{v}{3.6} \left(\frac{a}{3.6} + 9.81 \sin \theta \right) \quad (3.38)$$

where the above quantity is in kilowatt, the velocity v is in km/h, the acceleration/deceleration a is in km/h per second. θ denotes road degree. Post et al. (1984) also propose the following model of hydrocarbon (HC) emission rate for spark ignition vehicles

$$r^{\text{HC}}(t) = \begin{cases} 52.8 + 4.2Z & Z > 0 \\ 52.8 & Z \leq 0 \end{cases} \quad (3.39)$$

based on field experiments, where the hydrocarbon emission rate $r^{\text{HC}}(t)$ is in gram/hour, and Z is in kilowatt. The instantaneous fuel consumption-power relationship is

$$r^{\text{FC}}(t) = \begin{cases} 2.35 + 0.55Z & Z > 0 \\ 2.35 & Z \leq 0 \end{cases} \quad (3.40)$$

where the fuel consumption rate $r^{\text{FC}}(t)$ is in liter/hour, Z is in kilowatt.

4 Model Calibration

In order to address issues raised in Section 1.3, we propose to combine high-resolution vehicle trajectory data provided by NGSIM, with second-order traffic reconstruction techniques discussed in Section 3. A critical preliminary work is to calibrate the phase transition model in connection with the field data available for experimentation.

To this end, we consider the northbound of Interstate 80 located in Emeryville, CA. The highway segment of interest spans 1650 feet in length with an on-ramp at Powell Street and an off-ramp at Ashby Avenue. The highway segment has six lanes with the leftmost lane being a *high-occupancy vehicle* (HOV) lane. Data were collected using several video cameras. Digital video images were collected over an approximate five-hour period from 2:00 pm to 7:00 pm on April 13, 2005. Complete vehicle trajectories transcribed at a resolution of 1 frame per 0.1 second, along with vehicle type, lane identification etc., were recorded and processed over three time slots: 4:00 pm - 4:15 pm, 5:00 - 5:15 pm, and 5:15 - 5:30 pm. The layout of the study area is shown in Figure 1.

4.1 Temporal-spatial cells

We begin with estimating the density-flow relation needed for the congested phase of the PTM (1.2); the goal is to identify appropriate numerical values for the constants A and B mentioned in (3.10) and subsequent calculations. Notice that unlike the classical LWR model, where the density-flow relation is expressed as a function of one single variable, the fundamental diagram

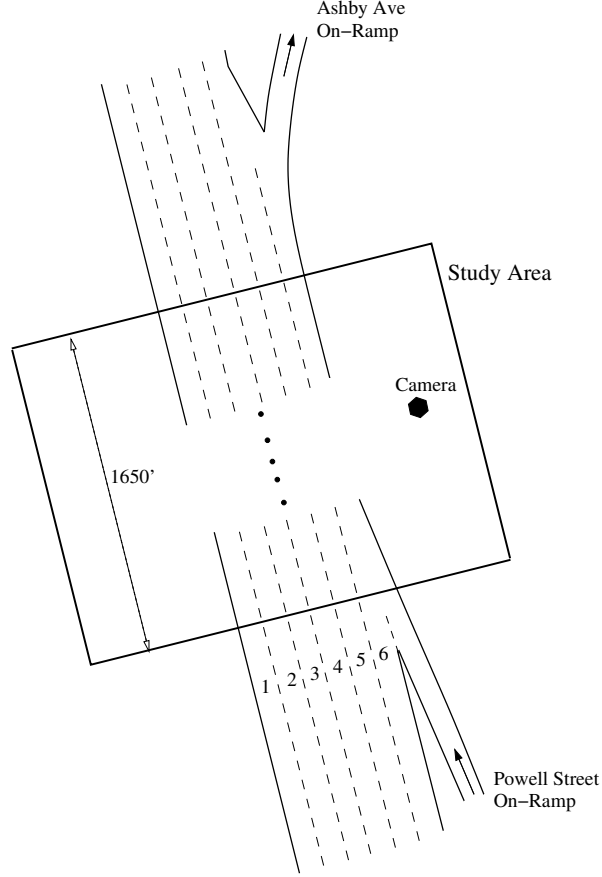


Figure 1: The study area spans 1650 feet in length in the northbound of Interstate 80 located in Emeryville, CA.

corresponding to the congested phase of PTM is a multi-valued map. This means that a given density ρ corresponds to a range of values of the flow $\rho \cdot v(\rho, q)$, $q \in [q_{min}, q_{max}]$. We note that vehicles using the HOV lane (#1) have a significantly higher average velocity than those in the other lanes, indicating the presence of uncongested condition. Thus we exclude lane # 1 from our estimation since we are mainly interested in the congested phase. We also remove lane # 6 to reduce the uncertainty due to merging and diverging traffic (see Figure 1).

In order to identify all the possible values of $v(\rho, q)$ in the NGSIM dataset for a given density value ρ , we partition the study area into cells expressed as spatial intervals $[x_i, x_{i+1}]$, $i \in 1, \dots, N_X - 1$. Let us also consider the temporal-spatial cells $C_{i,j}$, $i = 1, \dots, N_T$, $j = 1 \dots, N_X$, where i and j indicate the time step and spatial step, respectively. The average density of cell C_{ij} is estimated via the number of vehicles whose trajectories indicate the presence in $[x_i, x_{i+1}]$ during time $[t_i, t_{i+1}]$. While the average velocity is the arithmetic mean of all velocity measurements inside cell C_{ij} . Figure 2 illustrates such a procedure.

4.1.1 Numerical specifications

We use vehicle trajectory data collected at a 1/10 second resolution on an I-80 segment spanning 1650 feet in length. We consider the stretch in the middle from relative feet 50 to relative feet 1600. The time periods include 4:00 pm - 4:15 pm (2051 vehicles), 5:00 pm - 5:15 pm (1835 vehicles) and 5:15 pm - 5:30 pm (1789 vehicles). During each time period,

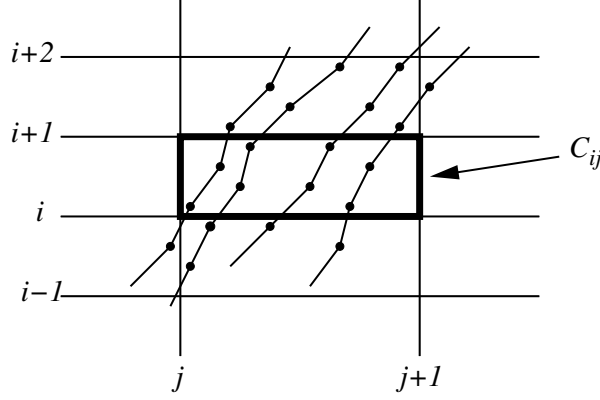


Figure 2: Estimation of density and velocity on a cell level. Curves with solid dots represent vehicle trajectories. The instantaneous velocities of cars are measured/calculated at the solid dots. For instance, the occupancy of cell C_{ij} is four; the average velocity is taken as the mean of velocity measures at the eight dots inside C_{ij} .

we truncate the first and last 100 seconds. We also remove data collected from the HOV lane (#1) and lane # 6 to avoid modeling uncertainty induced by the uncongested traffic and merging/diverging traffic. The dimension of the cells used to construct the density-flow relation in the congested phase is 400 (feet) \times 4 (seconds).

4.1.2 Constructing the congested region in the fundamental diagram

The flow inside cell C_{ij} is calculated as the product of average density and flow. The density-flow data plots for the time periods 4:00 pm - 4:15 pm and 5:00 - 5:15 pm are shown in Figure 4. The fundamental diagram obtained from the whole dataset is shown in Figure 4.

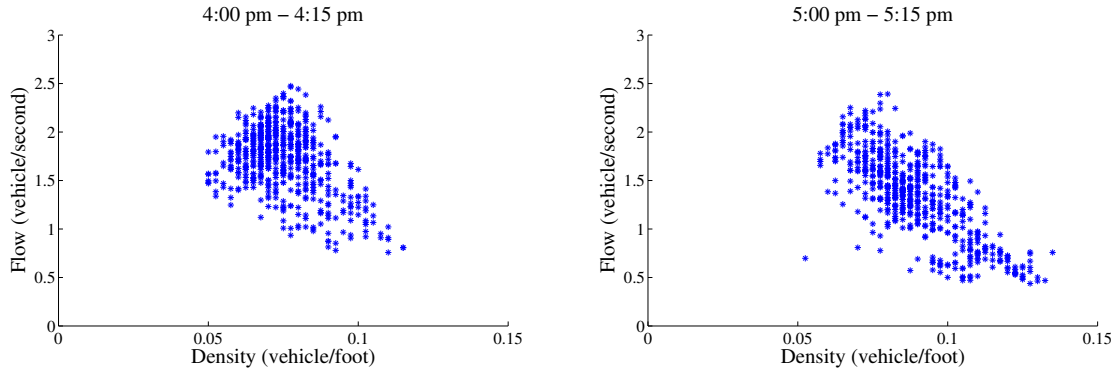


Figure 3: The fundamental diagram for the PTM expressed as a set-valued function of density.

Equation (3.10) suggests an affine density-velocity relation when the perturbation $q - q^*$ is zero. Notice that the perturbation can have different signs. We normalize $q - q^*$ such that $q - q^* \in [-1, 1]$. Therefore the upper and lower envelopes of the congested domain in the density-velocity relation depicted in Figure 4 are respectively

$$\begin{cases} A(\rho_{jam} - \rho) + B(\rho_{jam} - \rho) \\ A(\rho_{jam} - \rho) - B(\rho_{jam} - \rho) \end{cases}$$

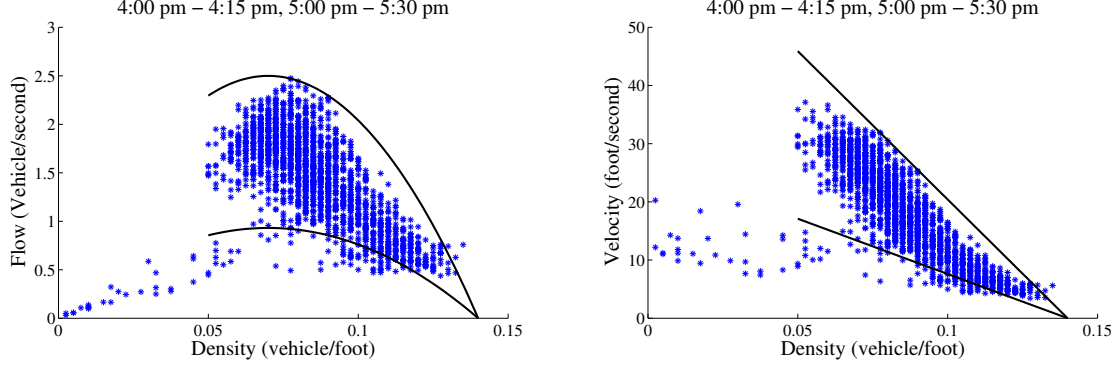


Figure 4: The fundamental diagram for the PTM expressed as a set-valued function of density.

Similarly, the upper and lower envelopes of the congested domain in the density-flow relation are

$$\begin{cases} A(\rho_{jam} - \rho)\rho + B(\rho_{jam} - \rho)\rho \\ A(\rho_{jam} - \rho)\rho - B(\rho_{jam} - \rho)\rho \end{cases}$$

We choose $A = 350$, $B = 160$. The corresponding congested regions are depicted as the areas formed by the black curves in Figure 4.

5 Estimating traffic quantities along vehicle trajectories

The vehicle trajectories in the raw data are recorded every 1/10 second. In order to test the effect of under sampling, we introduce the integer parameter N and approximate the vehicle trajectory by sampling every N data points. Since the sampling period of mobile devices is usually 3 seconds, a typical value of N is 30. For comparison purposes, we consider other values of N as well.

We follow the discussion in Section 2 and use the approximate trajectory data for estimating the following quantities along each vehicle trajectory:

$$\hat{\rho}(t, x(t)) \equiv \rho_{jam} - \rho(t, x(t)), \quad \hat{q}(t, x(t)) \equiv q(t, x(t)) - q^*$$

where $x(\cdot)$ denotes the trajectory of a given vehicle, ρ_{jam} is the jam density, the threshold parameter q^* distinguishes between possible behavior of the flow; see Colombo (2002a). More specifically, fix $N \geq 1$, let $t_i, i = 1, \dots, m$ be the time instances at which the location is recorded. Let $x(t_i), i = 1, \dots, m$ be the corresponding location of the vehicle. The basic quantities v , $\frac{Dv}{Dt}$ and v_x used to construct $\hat{\rho}$ and \hat{q} are estimated as follows.

$$v(t_i) \sim \frac{x(t_{i+1}) - x(t_{i-1}))}{2\delta t}, \quad \text{or} \quad v(t_i) \sim \frac{x(t_{i+1}) - x(t_i)}{\delta t} \quad (5.41)$$

$$\frac{Dv}{Dt}(t_i) \sim \frac{x(t_{i+1}) - 2x(t_i) + x(t_{i-1}))}{\delta t^2} \quad (5.42)$$

$$\frac{\partial}{\partial x} v \left(t_i, \frac{x(t_{i+1}) + 2x(t_i) + x(t_{i-1}))}{4} \right) \sim \frac{2}{\delta t} \cdot \frac{x(t_{i+1}) - 2x(t_i) + x(t_{i-1}))}{x(t_{i+1}) - x(t_{i-1}))} \quad (5.43)$$

Using the estimated values (5.41) - (5.43), we calculate $\hat{\rho} = \rho_{jam} - \rho$ (first-order) and $\hat{q} = q - q^*$ (second-order) following Section 3, for the following cases. For shorter notations,

we denote by v , $\frac{Dv}{Dt}$ and v_x the right hand sides of (5.41), (5.42) and (5.43), respectively.

(i) Phase transition model with source and strongly stable traffic:

$$\hat{\rho}(t_i, x(t_i)) = \frac{1}{A} \left(v + \frac{1}{3} \frac{Dv}{Dt} \right) \quad (5.44)$$

$$\hat{q}(t_i, x(t_i)) = -\frac{1}{3} \frac{A}{B} \frac{\frac{Dv}{Dt}}{v + \frac{1}{3} \frac{Dv}{Dt}} \quad (5.45)$$

Here in (5.45), the velocity v is estimated using either expression in (5.41), depending on whether or not the denominator $v + \frac{1}{3} \frac{Dv}{Dt}$ vanishes.

(ii) Phase transition model with source and less strongly stable traffic:

$$\hat{\rho}(t_i, x(t_i)) = v \frac{v + \frac{1}{3} \frac{Dv}{Dt}}{A(v + \frac{1}{3} v v_x)} \quad (5.46)$$

$$\hat{q}(t_i, x(t_i)) = -\frac{1}{3} \frac{A}{B} \frac{\frac{Dv}{Dt} - v v_x}{v + \frac{1}{3} \frac{Dv}{Dt}} \quad (5.47)$$

One needs to proceed cautiously with the right hand side of (5.47) since $\frac{Dv}{Dt} - v v_x$ may vanish under discrete-time approximation as shown by (3.27). Therefore, we calculate v according to

$$v(t_i) \sim \frac{x(t_{i+1}) - x(t_i)}{\delta t}$$

(iii) Phase transition model without source term. The feasibility of solutions of the quadratic equation (3.32) can be relatively easily analyzed in a discrete-time framework. First, we readily calculate that

$$\begin{aligned} \frac{1}{v_x} \frac{Dv}{Dt} &\sim \frac{\delta t}{2} \cdot \frac{x(t_{i+1}) - x(t_{i-1})}{x(t_{i+1}) - 2x(t_i) + x(t_{i-1}))} \cdot \frac{x(t_{i+1}) - 2x(t_i) + x(t_{i-1}))}{\delta t^2} \\ &= \frac{x(t_{i+1}) - x(t_{i-1}))}{2\delta t} \sim v(t_i) \end{aligned} \quad (5.48)$$

which is always positive. In light of this calculation, the feasibility condition (3.34) becomes

$$\frac{3}{2}v \geq \sqrt{A\rho_{jam}v} \quad (5.49)$$

that is,

$$v \geq \frac{4}{9} A\rho_{jam} \quad (5.50)$$

Using approximation (5.48), the discussion at the end of Section 3.1.3 reduces to the following:

- If $v > \frac{1}{2} A\rho_{jam}$, Then \hat{q} is computed as

$$\hat{q} = \frac{-B(2A\rho_{jam} - 3v) + \sqrt{\Delta}}{2B^2\rho_{jam}} \quad (5.51)$$

where

$$\Delta = B^2(9v^2 - 4A\rho_{jam}v)$$

ρ is computed accordingly as

$$\rho = \frac{1}{B\hat{q}}(2v - A\rho_{jam}) \quad (5.52)$$

- If $v \leq \frac{1}{2}A\rho_{jam}$, then \hat{q} is computed as

$$\hat{q} = \frac{-B(2A\rho_{jam} - 3v) - \sqrt{\Delta}}{2B^2\rho_{jam}} \quad (5.53)$$

ρ is computed according to (5.52).

Whenever the feasibility condition $v \geq \frac{4}{9}A\rho_{jam}$ does not hold, there are no real solutions of ρ and \hat{q} .

Finally, the estimated quantities $\hat{\rho}$ (or ρ) and \hat{q} depend not only on the types of traffic flow models and assumptions employed, but also on the value of N . In order to compare different cases on the same ground, we interpolate the continuous-time quantities such as $v(t)$, $\frac{Dv}{Dt}(t)$, $\hat{\rho}(t, x(t))$ and $\hat{q}(t, x(t))$ with piecewise affine functions. In order to assess the estimation error, we compute the relative L^1 error between the quantities obtained with $N > 1$, and the ones obtained with $N = 1$, i.e. the ground truth data.

5.1 Error of estimation due to under sampling

In this section, we present the estimation errors associated with various traffic quantities including velocity and acceleration (Section 5.1.1); $\hat{\rho}$ and \hat{q} (Section 5.1.2); and the power demand function which is closely related to vehicle emission and fuel consumption (Section 5.1.3). We will select different values of N to study the deterioration of estimation quality due to under sampling.

All the numerical results reported below are obtained via data from three time periods: 4:00 pm - 4:15 pm, 5:00 pm - 5:15 pm, and 5:15 pm - 5:30 pm. The numbers of vehicles involved in these three time periods are respectively 3366, 2872 and 3011.

5.1.1 Reconstructing velocity and acceleration profiles

As the most fundamental subject of our numerical study, the velocity and acceleration of the same vehicle, estimated from (5.41) and (5.42) with $N > 1$, are compared with the ground truth ($N = 1$). Following the steps explained immediately above, we compute and summarize the mean and standard deviation of the relative L^1 error, and present them in Table 1.

It is apparent from Table 1 that the estimation of the second order quantity (acceleration) is much more deteriorated by under sampling than that of the first order quantity (velocity). Such result coincides with intuition: the acceleration, as the derivative of velocity, has worsened regularity and higher variation. This is also confirmed in Figure 5 where the temporal trajectories of v and a are displayed with different values of N .

5.1.2 Reconstructing $\hat{\rho}$ and \hat{q}

The first-order quantity $\hat{\rho} = \rho_{jam} - \rho$ and the second-order quantity $\hat{q} = q - q^*$ are estimated by (5.44)-(5.45) when the traffic is strongly stable, by (5.46) -(5.47) when the traffic is less stable, and by (5.50)-(5.53) when there is no source term in the PTM.

In the numerical results below, we choose the following numerical values obtained from model calibration (Section 4.1)

$$A = 350, \quad B = 160, \quad \rho_{jam} = 0.14 \text{ (vehicle/foot)}$$

	Mean (%)				Standard deviation (%)			
Sampling period δt (s)	0.5	1	2	3	0.5	1	2	3
$\frac{\ v_{true} - v_{\delta t}\ _{L^1}}{\ v_{true}\ _{L^1}}$	3.27	4.72	6.36	7.58	1.50	1.81	2.31	2.87
$\frac{\ a_{true} - a_{\delta t}\ _{L^1}}{\ a_{true}\ _{L^1}}$	88.12	98.77	102.23	102.53	9.52	3.10	2.04	2.04

Table 1: Relative error using different sampling frequency. v_{true} denotes to the ground-truth data, while $v_{\delta t}$ is the approximated velocity by sampling every δt seconds.

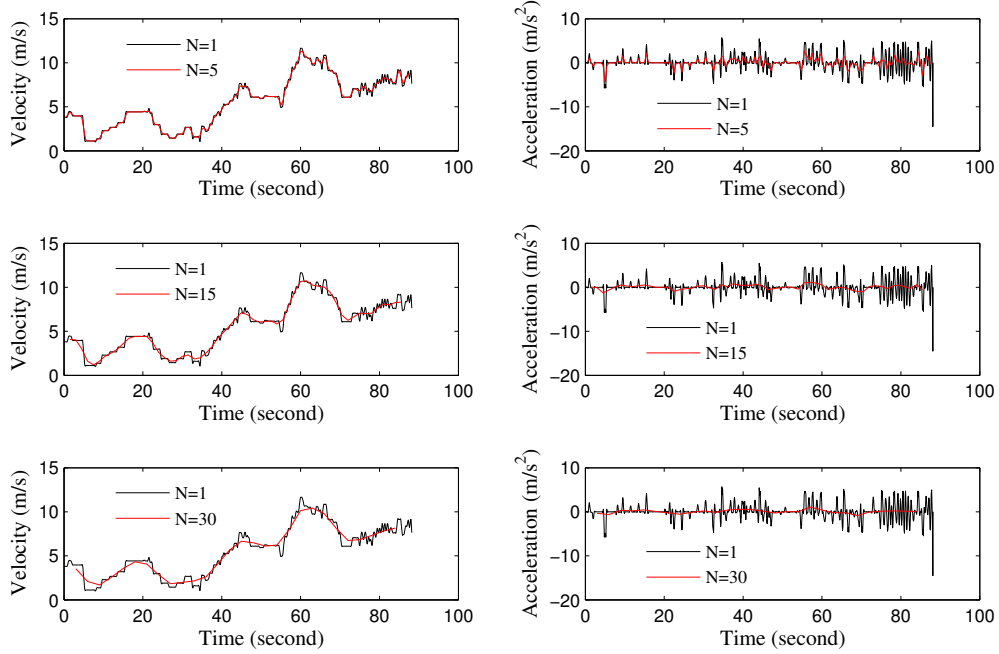


Figure 5: Ground-truth and estimated trajectories of velocity (left) and acceleration (right) of the same vehicle.

As we show in Figure 4, the maximum velocity of vehicles under study is below 30 mile/hour. Thus the use of the congested phase in the phase transition model is appropriate.

(i) PTM with source and strongly stable traffic.

The mean and standard deviation of the relative L^1 error are summarized in Table 2, where $\hat{\rho}_{true}(\cdot)$ denotes the ground truth obtained by the raw data; $\hat{\rho}_{\delta t}(\cdot)$ denotes the reconstructed data by choosing $N > 5, 10, 20$ and 30 , respectively. The notations involving q have similar meanings.

(ii) PTM with source and less stable traffic.

The mean and standard deviation of the relative L^1 error are summarized in Table 3.

We notice that for the phase transition model with source and less stable traffic, the error

		Mean (%)				Standard deviation (%)			
	δt (second)	0.5	1	2	3	0.5	1	2	3
4:00-4:15	$\ \hat{\rho}_{true} - \hat{\rho}_{\delta t}\ _{L^1}$	10.43	11.94	13.55	14.60	6.42	6.28	6.33	6.37
	$\ \hat{\rho}_{true}\ _{L^1}$								
	$\ \hat{q}_{true} - \hat{q}_{\delta t}\ _{L^1}$	104.51	101.29	102.33	102.27	64.91	5.85	2.94	2.74
	$\ \hat{q}_{true}\ _{L^1}$								
5:00-5:15	$\ \hat{\rho}_{true} - \hat{\rho}_{\delta t}\ _{L^1}$	6.21	8.64	11.44	13.30	1.58	2.28	3.31	4.17
	$\ \hat{\rho}_{true}\ _{L^1}$								
	$\ \hat{q}_{true} - \hat{q}_{\delta t}\ _{L^1}$	130.34	109.56	107.74	106.77	116.69	14.54	7.59	5.96
	$\ \hat{q}_{true}\ _{L^1}$								
5:15-5:30	$\ \hat{\rho}_{true} - \hat{\rho}_{\delta t}\ _{L^1}$	7.47	10.31	13.50	15.64	2.18	3.08	4.18	5.03
	$\ \hat{\rho}_{true}\ _{L^1}$								
	$\ \hat{q}_{true} - \hat{q}_{\delta t}\ _{L^1}$	148.74	114.59	109.12	107.47	196.54	17.00	8.70	6.81
	$\ \hat{q}_{true}\ _{L^1}$								

Table 2: Estimation based on phase transition model with source and strongly stable traffic.

		Mean (%)				Standard deviation (%)			
	δt (second)	0.5	1	2	3	0.5	1	2	3
4:00-4:15	$\ \hat{\rho}_{true} - \hat{\rho}_{\delta t}\ _{L^1}$	20.61	11.83	12.81	14.52	70.07	11.58	10.39	10.45
	$\ \hat{\rho}_{true}\ _{L^1}$								
	$\ \hat{q}_{true} - \hat{q}_{\delta t}\ _{L^1}$	436.42	713.14	544.32	502.82	484.40	860.39	669.68	631.80
	$\ \hat{q}_{true}\ _{L^1}$								
5:00-5:15	$\ \hat{\rho}_{true} - \hat{\rho}_{\delta t}\ _{L^1}$	11.05	10.21	11.69	14.17	16.79	13.64	10.81	10.37
	$\ \hat{\rho}_{true}\ _{L^1}$								
	$\ \hat{q}_{true} - \hat{q}_{\delta t}\ _{L^1}$	858.51	639.31	512.63	462.53	874.62	625.31	498.05	423.06
	$\ \hat{q}_{true}\ _{L^1}$								
5:15-5:30	$\ \hat{\rho}_{true} - \hat{\rho}_{\delta t}\ _{L^1}$	15.37	14.11	15.51	18.08	20.50	18.88	16.77	15.97
	$\ \hat{\rho}_{true}\ _{L^1}$								
	$\ \hat{q}_{true} - \hat{q}_{\delta t}\ _{L^1}$	590.76	435.68	359.03	337.78	601.29	417.20	300.95	278.43
	$\ \hat{q}_{true}\ _{L^1}$								

Table 3: Estimation based on phase transition model with source and less stable traffic.

for second-order quantity \hat{q} is huge. This mainly stems from the fact that the L^1 norm of the ground truth \hat{q}_{true} is very small. Recall (5.47)

$$\hat{q} = -\frac{1}{3} \frac{A}{B} \frac{\frac{Dv}{Dt} - vv_x}{v + \frac{1}{3} \frac{Dv}{Dt}}$$

and identity (3.27), we see that the \hat{q} is very close (if not identical) to zero, even if slightly different approximation schemes of v , v_x and $\frac{Dv}{Dt}$ are adapted. This explains the small L^1 norm of \hat{q}_{true} and large relative error.

(iii) PTM without source.

As we show in our calculation (5.50)-(5.53), the model has a feasible solution if and only if $v > 4/9 A \rho_{jam} \approx 21.8$ (feet/second). For simplicity, in our computation we only select

those vehicles with velocities uniformly above 21.8 (feet/second). A more thorough approach would be to utilize all partial trajectories that yield velocities above 21.8 (feet/second), this is however, not the focus of this paper.

Under such rather restrictive criteria mentioned above, the results of relative error are summarized in Table 4. We note that among all three time periods, only a total of 36 vehicles are selected. Therefore, although the errors displayed in Table 4 are quite small, such a computational procedure is limited in practice if the prevailing velocity is very low, unless the vehicle trajectories are utilized in a piecewise manner.

	δt (second)	Mean (%)				Standard deviation (%)			
		0.5	1	2	3	0.5	1	2	3
4:00-4:15	$\ \hat{\rho}_{true} - \hat{\rho}_{\delta t}\ _{L^1}$	0.96	1.27	1.50	1.65	1.10	1.49	1.59	1.51
	$\ \hat{\rho}_{true}\ _{L^1}$								
	$\ \hat{q}_{true} - \hat{q}_{\delta t}\ _{L^1}$	6.17	9.29	12.37	14.47	3.09	4.58	6.04	7.11
	$\ \hat{q}_{true}\ _{L^1}$								
5:00-5:15	$\ \hat{\rho}_{true} - \hat{\rho}_{\delta t}\ _{L^1}$	0.65	1.43	2.82	3.23	0.63	1.61	3.26	3.65
	$\ \hat{\rho}_{true}\ _{L^1}$								
	$\ \hat{q}_{true} - \hat{q}_{\delta t}\ _{L^1}$	3.93	6.82	11.35	14.30	1.77	3.52	6.40	7.73
	$\ \hat{q}_{true}\ _{L^1}$								
5:15-5:30	$\ \hat{\rho}_{true} - \hat{\rho}_{\delta t}\ _{L^1}$	0.45	0.66	0.84	0.92	0.17	0.15	0.14	0.20
	$\ \hat{\rho}_{true}\ _{L^1}$								
	$\ \hat{q}_{true} - \hat{q}_{\delta t}\ _{L^1}$	4.97	8.34	10.60	11.60	1.34	2.21	2.82	3.00
	$\ \hat{q}_{true}\ _{L^1}$								

Table 4: Estimation based on phase transition model without source.

5.1.3 Reconstructing emission and fuel consumption rates

We use the modal-based model (Post et al., 1984) to calculate the total power function and associated emission rate and fuel consumption rate. The computation involves car speed v and acceleration $\frac{Dv}{Dt}$, which are estimated according to (2.7) and (2.8).

δt (second)	Mean (%)				Standard deviation (%)			
	0.5	1	2	3	0.5	1	2	3
$\ Z_{true} - Z_{\delta t}\ _{L^1}$	78.78	94.49	99.08	99.49	8.91	3.31	2.20	2.08
$\ Z_{true}\ _{L^1}$								
$\ r_{true}^{HC} - r_{\delta t}^{HC}\ _{L^1}$	30.42	35.88	37.10	36.69	16.09	16.97	17.15	17.10
$\ r_{true}^{HC}\ _{L^1}$								
$\ r_{true}^{FC} - r_{\delta t}^{FC}\ _{L^1}$	47.27	56.29	58.67	58.41	16.03	16.11	16.21	16.30
$\ r_{true}^{FC}\ _{L^1}$								

Table 5: Estimation of emission and fuel consumption along vehicle trajectories. Z : power demand; r^{HC} : hydrocarbon emission rate; r^{FC} : fuel consumption rate.

Table 5 summarizes the error in estimating the power demand, emission rates and fuel consumption rate under different sampling frequency. In general, estimations of these higher-order road quantities suffer from under sampling. However, the estimation of certain quantity

such as r^{HC} can be relatively accurate. This can be somehow explained by (3.38)-(3.40): the affine power-emission relationship for hydrocarbon shown in (3.39) has a large y -intercept and relatively small slope, making the emission rate less sensitive to the error in Z . Finally, it is not surprising that the power demand Z cannot be accurately estimated since it directly involves second-order quantities such as acceleration/deceleration. These subtleties can be visualized in Figure 6, which show the trajectories of these quantities associated with a single car.

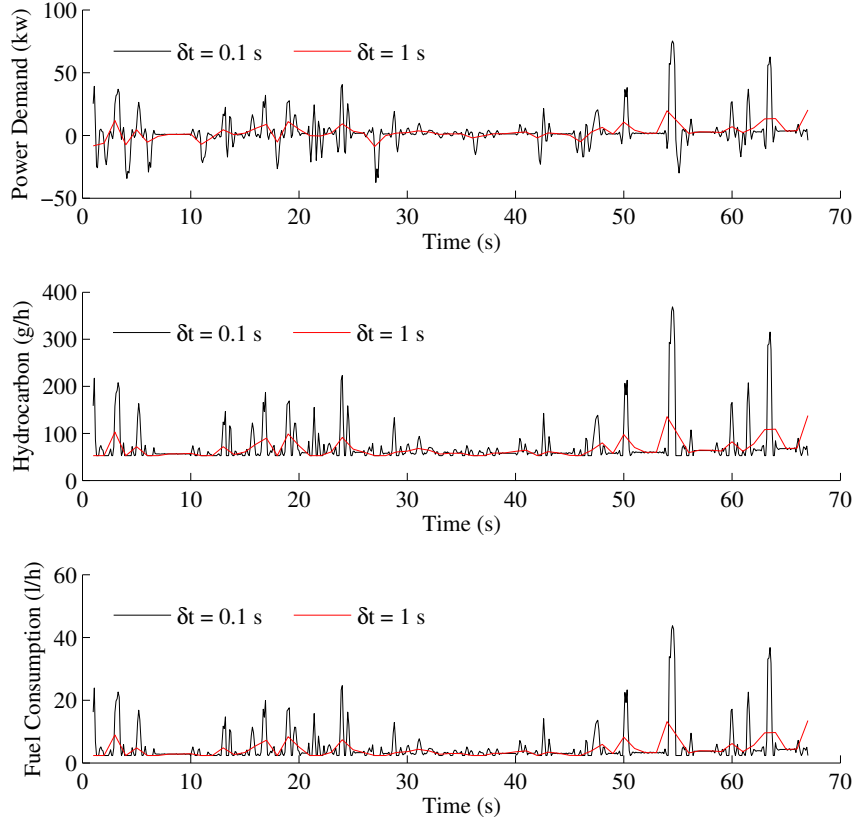


Figure 6: Ground truth and reconstructed trajectories for power demand (top), hydrocarbon emission rate (middle), and fuel consumption (bottom).

6 Reconstructing Eulerian Quantities

In the previous section, we are mainly concerned with first- and higher-order quantities associated with a fixed vehicle; in other words, they are quantities fixed in the Lagrangian coordinates. It is natural to explore the effect of under sampling of vehicle locations in an Eulerian framework; we are also prompted to examine how the estimating error depends on the vehicle penetration rate.

6.1 Calculating cell-based $\hat{\rho}$

We consider each temporal-spatial cell C_{kl} , $k = 1, \dots, N_T$, $l = 1, \dots, N_X$ expressed as a product of intervals $[\tau_k, \tau_{k+1}] \times [x_l, x_{l+1}]$. In a similar way as Section 4.1, we consider all the location measurements in the dataset that fall within the cell C_{ij} . Recall that given a discrete-time trajectory of a vehicle:

$$\dots, x(t_{i-1}), x(t_i), x(t_{i+1}), \dots$$

where $\{t_i\}$ is a fixed time grid, we can estimate the velocity $v(t_i)$ and acceleration $a(t_i)$ as well as the Lagrangian density $\hat{\rho}(t_i, x(t_i))$ using techniques mentioned in Section 2. In order to calculate $\hat{\rho}$ inside cell C_{kl} , we search for vehicles whose trajectory intersect C_{kl} , and the quantity $\hat{\rho}_{kl}$ associated with the cell C_{kl} is estimated as the mean of all $\hat{\rho}(t_j, x(t_j))$ such that $(t_j, x(t_j)) \in [\tau_k, \tau_{k+1}] \times [x_l, x_{l+1}]$.

An example of such calculation is presented in Figure 7. We utilize dataset during 4:00 pm and 4:15 pm on I-80. The estimated density on the whole $t - x$ plane consisting of individual densities $\rho_{kl} \equiv \rho_{jam} - \hat{\rho}_{kl}$ is compared with the ground truth density profiled which is obtained by simply counting the number of vehicles present in a given cell. The advantage of our proposed method for estimating $\hat{\rho}$ is that it can be used to reconstruct the density (or velocity) profile when the penetration rate of probe vehicles is low, typically around 10%. This is the main subject of investigation in the next section.

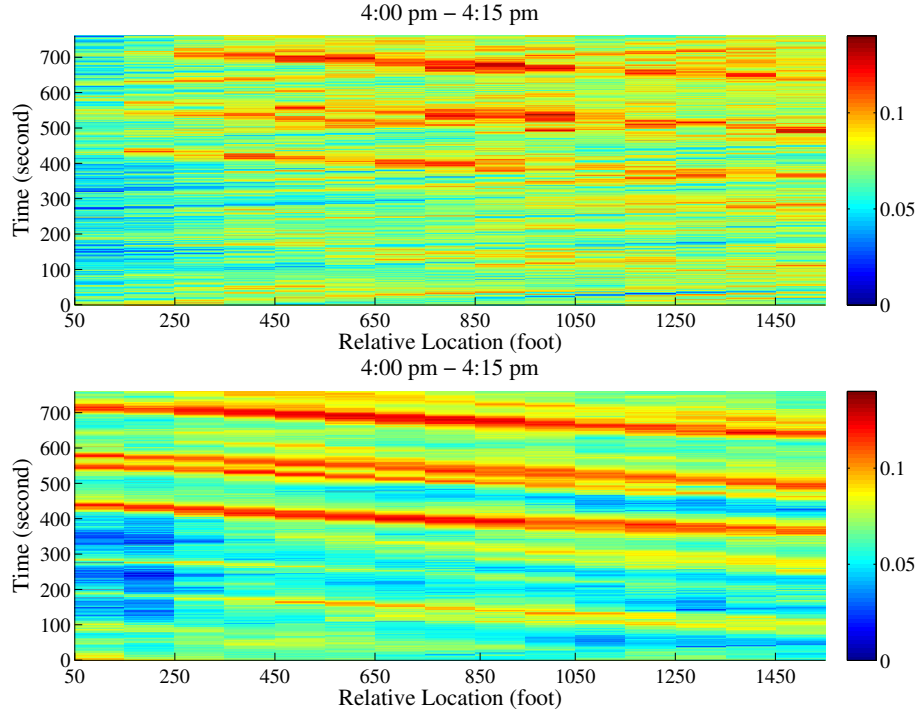


Figure 7: Reconstruction of cell densities (in vehicle/foot) during 4:00 pm - 4:15 pm. The upper panel shows the ground truth density obtained by counting the number of cars present in each cell during each time interval. The lower panel is the computational result with techniques described in Section 3 and 6.1.

6.2 Estimating density when the probe penetration rate is low

Traffic monitoring and data collection are often constrained by the coverage and penetration rate of sensors. In the case of Lagrangian sensing, that is, in the presence of mobile sensors such as smart phones or GPS, a low penetration rate is consistently a major hurdle to real-time traffic estimation and prediction. In the analysis that follows, we are concerned with finding an appropriate range of penetration rates such that the domain of study is covered while the estimation error remain reasonably low.

The procedure of estimating cell densities is very similar to that described in Section 6.1 except with fewer vehicle trajectories. Furthermore, in choosing the size of the cells, one should take into consideration the following two factors: 1) to capture sufficient samples for averaging purpose, the dimension of a spatial cell should ideally be on the scale of one hundred meters; 2) when the size of a cell is too small, the chance of having no measurements therein is high. In light of these two points, we choose the spatial size of a cell to be 400 feet (≈ 120 meters).

We take several factors into our consideration.

- The sampling period (in second) is the time between two consecutive recordings of a vehicle location. A typical sampling period of mobile sensors (GPS) is three to four seconds. Recall that the NGSIM dataset has a 0.1 sampling period, which is considered the ground truth in our calculation.
- The penetration rate of probe vehicles. The following values are considered: 100%, 20%, 10%, 5% and 2%. The probe vehicles are chosen such that they are evenly distributed in the traffic stream.
- Modeling assumptions. We consider both strongly stable traffic and less stable traffic.

Numerical results are summarized in Table 6 when the traffic stream is assumed to be strongly stable. The results contain three time periods: 4:00-4:15 pm, 5:00-5:15 pm and 5:15-5:30 pm. The main variables are the sampling period and the penetration rate. The ground truth is computed with a sampling period of 0.1 second and 100% penetration rate. The coverage rate of a given penetration rate is computed as the ratio between the number of cells that have at least one measurement in it (we call such a cell active) and the total number of cells. Finally, the average relative error of cell densities are calculated among all active cells. The same calculation is repeated when the traffic is assumed to be less stable, and the results are shown in Table 7.

From both cases, we notice that the penetration rate of probe vehicles has a substantial effect on the accuracy of our estimation; while the sampling period plays only a minor role. The modeling assumptions of strongly and less strongly stable traffic yield qualitatively similar behaviors. We also observe that a penetration rate around 10% yields both good coverage rate ($\geq 97\%$) and satisfactory accuracy (error $\leq 20\%$).

An intuitive visualization of the cell-based density estimation is presented in Figure 8, when the penetration rate is 10% and sampling period is 3 seconds. Our method remains relatively accurate under low penetration rate and in the presence of several inactive cells (with no measurements) colored dark blue.

6.3 Estimating cell-based emission and fuel consumption rates

We have shown in Section 5.1.3 that the estimation of the power demand function, and emission/fuel consumption rates is largely deteriorated by insufficient sampling. We note that

			Probe Vehicle Penetration Rate				
		Sampling Period (s)	100 %	20 %	10 %	5 %	2 %
4:00-4:15	Average Error (%)	1	0.66	9.53	13.30	18.75	23.92
		2	1.32	9.34	12.97	18.41	23.82
		3	2.22	9.80	13.38	18.34	22.13
	Coverage Rate		100.00 %	99.42 %	97.69 %	87.50 %	45.38 %
5:00-5:15	Average Error (%)	1	0.70	11.47	19.92	30.31	39.70
		2	1.50	11.65	19.16	29.72	38.80
		3	2.75	11.90	19.68	29.04	37.12
	Coverage Rate		100.00 %	100.00 %	98.79 %	88.91 %	49.40 %
5:15-5:30	Average Error (%)	1	0.73	12.00	17.87	25.34	39.68
		2	1.58	11.77	17.70	25.25	38.85
		3	2.96	12.04	17.60	24.66	36.58
	Coverage Rate		100.00 %	100.00 %	99.85 %	96.22 %	59.88 %

Table 6: Results of density estimation using different sampling periods and penetration rates, when the traffic is assumed to be strongly stable.

			Probe Vehicle Penetration Rate				
		Sampling Period (s)	100 %	20 %	10 %	5 %	2 %
4:00-4:15	Average Error (%)	1	1.32	9.47	13.13	17.97	23.45
		2	2.67	9.75	13.33	18.07	23.96
		3	4.18	10.88	14.38	19.23	23.40
	Coverage Rate		100.00 %	99.42 %	97.69 %	87.31 %	45.19 %
5:00-5:15	Average Error (%)	1	1.51	10.87	18.76	27.37	35.32
		2	3.22	11.27	18.71	27.97	35.37
		3	4.96	12.24	19.80	28.31	35.70
	Coverage Rate		100.00 %	100.00 %	98.79 %	88.31 %	47.98 %
5:15-5:30	Average Error (%)	1	1.85	10.98	16.39	22.73	33.22
		2	4.20	11.79	17.67	24.15	34.44
		3	6.29	13.00	18.51	24.81	34.18
	Coverage Rate		100.00 %	100.00 %	99.85 %	95.78 %	57.70 %

Table 7: Results of density estimation using different sampling periods and penetration rates, when the traffic is assumed to be less strongly stable.

such significant error is caused by the high variation in the acceleration profile, see Figure 5 for an illustration. We also observe from Figure 6 that although higher-order fluctuations are averaged out, the estimated quantities using larger δt yield a good approximation in the average sense, that is, they provide relatively accurate estimation of the area under the curve. With this in mind, in this section we re-examine the estimation error on a cell level instead of along each vehicle trajectory. It is our expectation that, by averaging several data points in the same cell, one could come up with a better estimation of these higher order quantities.

Our methodology and numerical setup is similar to those in previous sections, and are

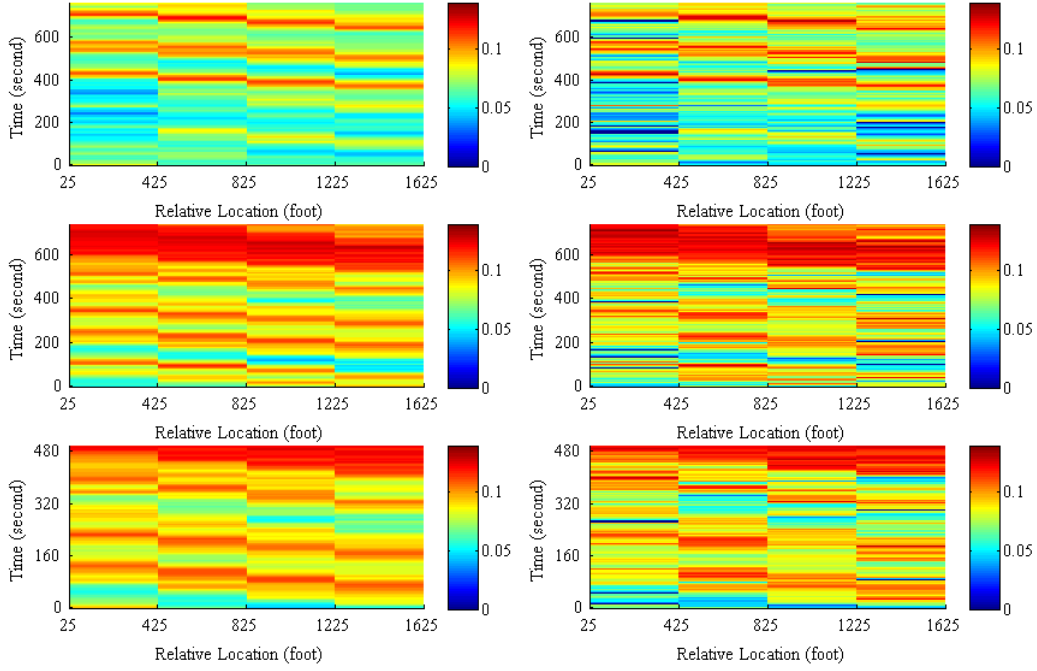


Figure 8: A comparison of the ground truth cell densities (left column) and the reconstructed cell densities (right column) with 10% penetration rate and 3 seconds sampling period. The three rows represent, from top to bottom, periods of 4:00-4:15 pm, 5:00-5:15 pm and 5:15-5:30 pm, respectively.

omitted for brevity. The numerical results are summarized in Table 8. The results show improved accuracy of estimation, compared to the estimation along single vehicle trajectories (see Table 5 for a comparison). Such observation coincides with our earlier observation that the reconstructed emission or fuel consumption rates, when δt is large, approximates the mean value of the ground truth well even though higher-order variations are ignored.

To further aggregate the emission and fuel consumption rates, we compute the total emission rate inside each temporal-spatial cell by multiplying cell density (in vehicle/foot) by unit emission/fuel consumption rate (in gram/hour per vehicle or liter/hour per vehicle). Then we sum up the emission/fuel consumption rates over all cells in the same time interval to get the total emission rate of the road segment of interest. Such time-dependent rates are plotted in Figure 9, where the ground-truth is compared with the estimation obtained from three-second sampling period (the same as GPS) and 10% probe penetration rate. From these figures we conclude that our estimation accurately captures the overall trends of emission and fuel consumption rates, although it tends to underestimate the true value since the three-second sampling period ignores higher-order variations in velocity and acceleration.

We further measure the relative error of the estimated hydrocarbon emission rate and the actual emission rate on this road segment, which has a mean value of 19.11% and a standard deviation of 10.89%; the mean of estimation error for fuel consumption is 32.12%, with a standard deviation 14.80%.

			Probe Vehicle Penetration Rate			
		Sampling Period (s)	100 %	50 %	20 %	10 %
5:00-5:30	r^{HC}	0.5	8.31	10.97	16.86	24.02
	Average	1	11.66	13.44	17.94	24.09
	Error (%)	2	14.49	15.95	19.45	24.35
		3	15.97	17.26	20.74	25.54
	Coverage Rate		100.00 %	100.00 %	99.42 %	97.69 %
5:00-5:30	r^{FC}	0.5	15.66	17.29	23.41	31.47
	Average	1	21.89	22.64	26.38	32.57
	Error (%)	2	26.97	27.54	29.94	34.04
		3	29.28	29.77	31.98	35.97
	Coverage Rate		100.00 %	100.00 %	99.42 %	97.69 %

Table 8: Estimation of r^{HC} and r^{FC} using different sampling periods and penetration rates, when the traffic is assumed to be strongly stable.

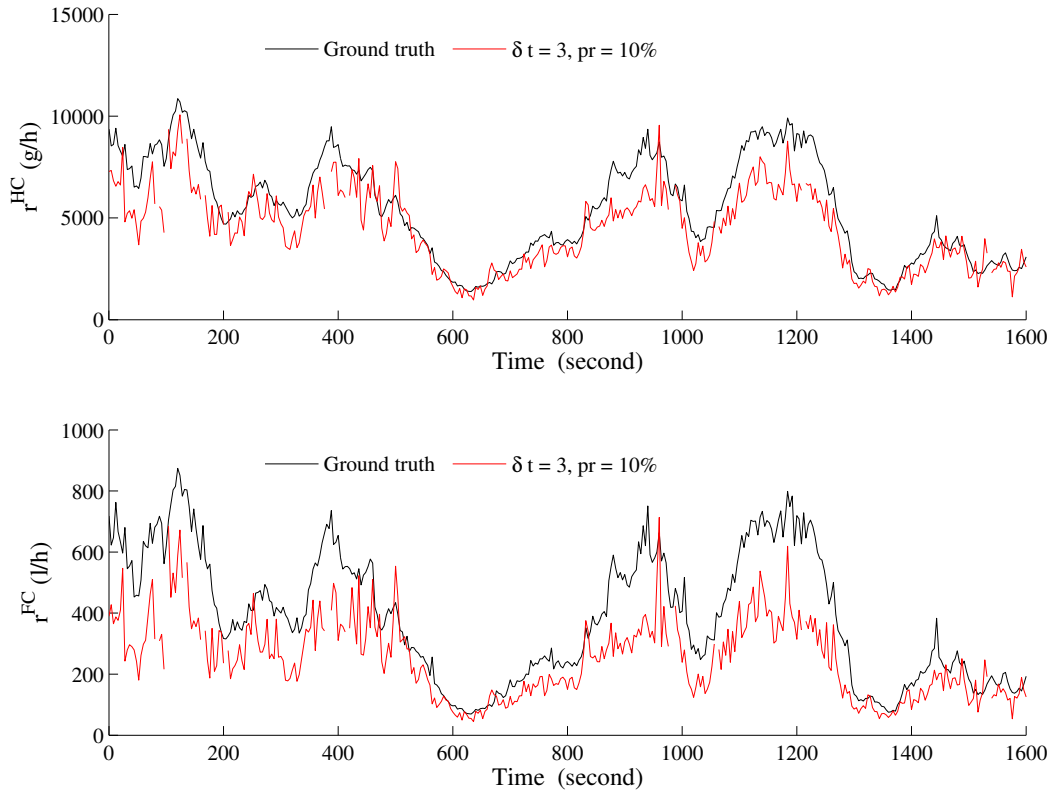


Figure 9: Time-varying emission and fuel consumption rates on the whole study area (1600 feet in length) for time period 5:00 - 5:30 pm. r^{HC} : emission rate of hydrocarbon in gram/hour; r^{FC} : fuel consumption rate in liter/hour. Red curve denotes the estimation based on three second sampling period and 10 % penetration rate.

6.3.1 Correction factors

Our previous numerical results reveal discernible estimation errors for emission and fuel consumption, despite the fact that the overall time-varying trends of these quantities are captured using our computational paradigm. As commented before, these errors are inevitable since the current sensing technology has insufficient sampling frequency due to limited development of cyberinfrastructure. One obvious way out of this is to increase the sampling frequency of existing mobile sensors or to deploy more probe sensors in the traffic stream, which requires technological advancement and is beyond the scope of this paper. Instead, we propose in this paper a correction factor approach for calibrating our estimation results using GPS readings (3 seconds) and low penetration rates (10 %).

We employ a linear regression approach that finds an appropriate affine relationship between the ground truth value and the estimated value. For both quantities of interest, r^{HC} and r^{FC} , we plot the ground-truth measurement versus the corresponding estimation on the same plane. Note that all these quantities are for the whole road segment. Figure 10 shows the approximate affine relationship between the ground truth value and the estimated one, for hydrocarbon emission and fuel consumption.

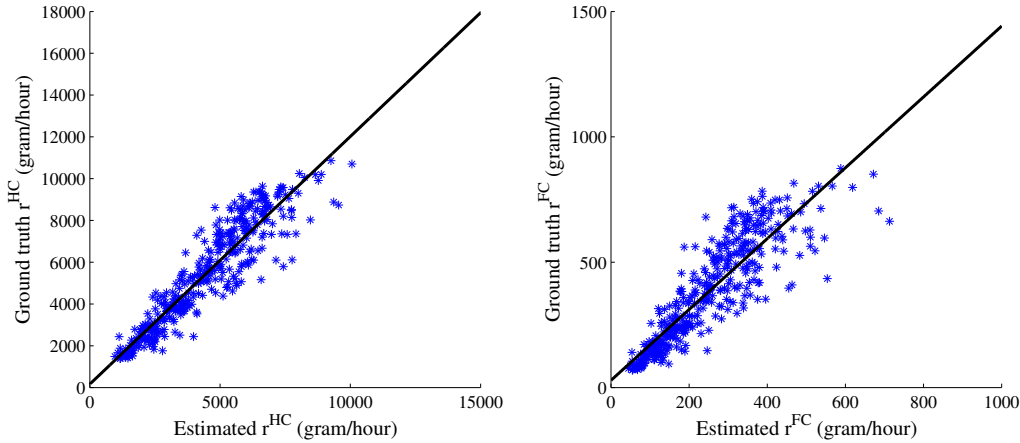


Figure 10: The approximate affine relationship between the ground truth value and the estimated one using 3 seconds sampling period and 10 % penetration rate. Left: r^{HC} in gram/hour. Right: r^{FC} in liter/hour.

We denote by r_{gt} the ground truth quantity, and by r_{es} the estimated quantity. The linear regression model assumes that $r_{gt} = \beta_0 + \beta_1 r_{es}$, $\beta_0, \beta_1 \in \mathbb{R}$. Data utilized for such linear regression is treated as training data. To be assured of the validity and robustness of the proposed affine adjustment, we employ a k -fold cross validation to be discussed below.

6.3.2 k -fold cross validation

We partition available vehicle trajectories into k equal size subsets. Of the k subsets, a single subset is used as the training data to obtain the linear coefficients β_0 and β_1 . The rest of the $k - 1$ subsets are used to validate the affine adjustment. Such procedure is repeated k times, each with distinct training dataset. Since we are focusing on a 10% penetration rate, it is natural to choose $k = 10$.

We compute the absolute relative error e_{abs} and the relative error e_{rel} as follows:

$$e_{abs} = \frac{|r_{es} - r_{gt}|}{|r_{gt}|}, \quad e_{rel} = \frac{r_{es} - r_{gt}}{|r_{gt}|}$$

where r_{es} denotes the estimation, r_{gt} denotes the ground truth. The result of the 10-fold cross validation is summarized in Table 9. It is quite clear from these results that applying the correction factor yields improved estimation accuracy. Figure 11 shows the corrected estimations of hydrocarbon and fuel consumption obtained by some test data, with correction factors given by the training data. We also run an informal normality test of the relative error e_{rel} by looking at the resulting histograms, which are depicted in Figure 12. The error roughly follow a normal distribution centered around 0.

	Hydrocarbon		Fuel consumption	
	Mean (%)	Std (%)	Mean (%)	Std (%)
e_{abs}	13.70	12.33	23.34	21.75
e_{rel}	-3.62	18.07	-10.06	30.28

Table 9: Cross validation results: Mean and standard deviation of estimation error with correction factors.

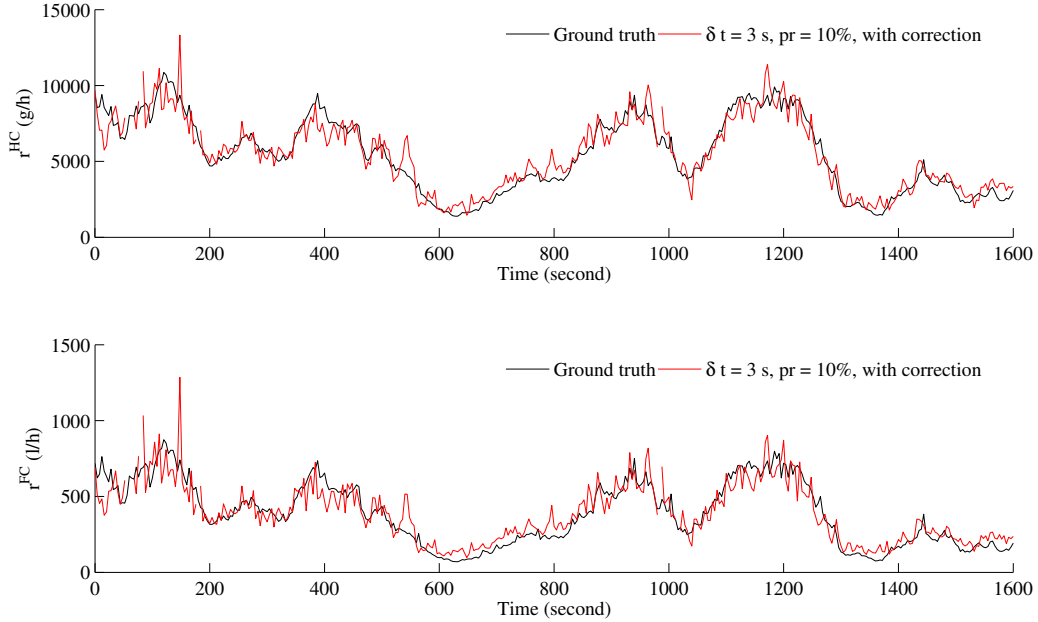


Figure 11: Emission and fuel consumption rates after the correction. Red curve denotes the corrected estimation of hydrocarbon emission r^{HC} and fuel consumption r^{FC} , based on three second sampling period and 10 % penetration rate, and a correction factor obtained from the training data.

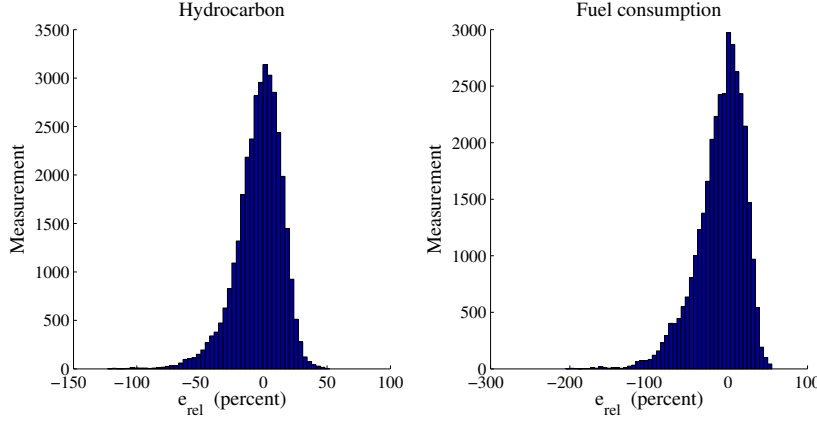


Figure 12: Histograms of the error e_{rel} .

7 Conclusion

In GPS-enabled mobile sensing paradigm, two factors are of pivotal importance: the probe penetration rate and the sampling frequency. The former has been emphasized multiple times in existing literature. It is our contention, established and proven in this paper, that sampling frequency of mobile devices also has a major impact on the quality of estimating higher-order traffic quantities such as acceleration, emission rate and fuel consumption rate. In particular, we have demonstrated the following:

- Various Eulerian (fixed-location) and Lagrangian (fixed-car) traffic quantities can be estimated via vehicle trajectory data, when the Phase Transition Model is employed.
- For both Lagrangian and Eulerian estimation, first-order quantities are accurately reconstructed by the proposed method.
- For second-order traffic quantities, under-sampling has a great impact on the estimation quality. The error is inevitable since the prevailing 3-second sampling period overlooks higher-order variations.
- The underestimation of hydrocarbon emission and fuel consumption rates can be corrected by imposing an affine correction factor that yields relatively accurate and robust estimation results.

Notes should be taken on the following important facts:

- Some numerical results presented herein should be interpreted only in comparison with each other. They do not necessarily reflect the real-world situation. For example, the estimation of emission and fuel consumption depends on each vehicle's characteristic such as type, make, etc., not just on its driving modes. It is for the purpose of extracting qualitative insights that simplified formulae such as (3.38)-(3.40) are employed.
- The traffic reconstruction approach presented by this paper does not directly address data error. However, qualitative results remain valid.

- The proposed correction factor for emission and fuel consumption is a potentially practical method that enhances GPS-based estimation. This method needs to be carefully calibrated in close view of road characteristics, type of vehicles, probe penetration rate and other relevant factors.

References

- Federal Highway Administration. Next Generation Simulation, 2006. <http://ngsim-community.org/>
- Aw, A., Rascle, M., 2000. Resurrection of “second order” models of traffic flow. *SIAM Journal on Applied Mathematics* 60, 916-938.
- Barth, M., An, F., Norbeck, J., Ross, M., 2007. Modal emission modeling: A physical approach. *Transportation Research Record* 1520, 81-88.
- Blandin, S., Argote, J., Bayen, A., Work, D., 2012. A phase transition model of non stationary traffic flow: Definition, properties and solution method. *Transportation Research Part B* 52, 31-55.
- Chan, C.C., 1997. An overview of power electronics in electric vehicles. *IEEE Transactions on Industrial Electronics* 44 (1), 3-13.
- Claudel, C.G., Bayen, A.M., 2010. Lax-Hopf based incorporation of internal boundary conditions into Hamilton-Jacobi equation. Part I: Theory. *IEEE Transactions on Automatic Control* 55 (5), 1142-1157.
- Claudel, C.G., Bayen, A.M., 2010. Lax-Hopf based incorporation of internal boundary conditions into Hamilton-Jacobi equation. Part II: Computational methods. *IEEE Transactions on Automatic Control* 55 (5), 1158-1174.
- Colombo, R.M., 2002a. Hyperbolic phase transitions in traffic flow. *SIAM Journal on Applied Mathematics* 63 (2), 708-721.
- Colombo, R.M., 2002b. On a 2×2 hyperbolic traffic flow model. *Math. Comput. Modeling* 35, 683-688.
- Colombo, R.M., Corli, A., 2002. Sonic hyperbolic phase transition and Chapman-Jouguet detonations, *Journal of Differential Equations*, 184, 321-347.
- Colombo, R.M., Goatin, P., Priuli, F.S., 2007. Global well posedness of traffic flow models with phase transitions. *Nonlinear Analysis* 66, 2413-2426.
- Daganzo, C.F., 1994. The cell transmission model. Part I: A simple dynamic representation of highway traffic. *Transportation Research Part B* 28 (4), 269-287.
- Daganzo, C.F., 1995. The cell transmission model. Part II: Network traffic. *Transportation Research Part B* 29 (2), 79-93.
- Demers, A., List, G.F., Wallace, W.A., Lee, E.E., Wojtowicz, J.M., 2006. Probes as path seekers: a new paradigm. *Transportation Research Record: Journal of the Transportation Research Board* 1944, 107114.

- Goatin, P., 2006. The Aw-Rascle vehicular traffic flow model with phase transitions. *Mathematics of Computation* 44, 287-303.
- Kwon, J., McCullough, B., Petty, K., Varaiya, P., 2007. Evaluation of PeMS to Improve the Congestion Monitoring Program. California PATH Research Report UCB-ITS-PRR-2007-6, Institute of Transportation Studies, University of California, Berkeley, CA.
- Lighthill, M., Whitham, G., 1955. On kinematic waves. II. A theory of traffic flow on long crowded roads. *Proceedings of the Royal Society of London. Series A, Mathematical and Physical Sciences* 229 (1178), 317-345.
- Herrera, J.C., Work, D.B., Herring, R., Ban, X.J., Jacobson, Q., Bayen, A., 2010. Evaluation of traffic data obtained via GPS-enabled mobile phones: The Mobile Century field experiment. *Transportation Research Part C* 18 (4), 568-583.
- Payne, H.J., 1971. Models of freeway traffic and control. Simulation Council.
- Payne, H.J., 1979. FREFLO: a macroscopic simulation model of freeway traffic. *Transportation Research Record*, 722 (1979), 68-75.
- Post, K., Kent, J.H., Tomlin, J., Carruthers, N., 1984. Fuel consumption and emission modelling by power demand and a comparison with other models. *Transportation Research Part A* 18 (3), 191-213.
- Richards, P.I., 1956. Shockwaves on the highway. *Operations Research* 4 (1), 42-51.
- Siebel, F., Mauser, W., 2006a. On the fundamental diagram of traffic flow, *SIAM Journal on Applied Mathematics* 66 (4), 1150-1162.
- Siebel, F., Mauser, W., 2006b. Synchronized flow and wide moving jams from balanced vehicular traffic, *Physical Review E*, DOI: 10.1103/PhysRevE.73.066108.
- Wang, Y., Papageorgiou, M., 2005. Real-time freeway traffic state estimation based on extended Kalman filter: A general approach. *Transportation Research Part B* 39 (2), 141-167.
- Whitham, G.B., 1974. *Linear and Nonlinear Waves*, Pure and Applied Mathematics, Wiley-Interscience, New York.
- Work, D. B., Blandin, S., Tossavainen, O. P., Piccoli, B., Bayen, A.M. (2010). A traffic model for velocity data assimilation. *Applied Mathematics Research eXpress*, 2010 (1), 1-35.
- Yim, Y., Cayford, R., 2001. Investigation of Vehicles as Probes using Global Positioning System and Cellular Phone Tracking: Field Operational Test. California PATH Working Paper UCB-ITS-PWP-2001-9, Institute of Transportation Studies, University of California, Berkeley, CA.
- Yuan, Y., Van Lint, J.W.C., Hoogendoorn, S. P., Vrancken, J. L. M., Schreiter, T. (2011). Freeway traffic state estimation using extended Kalman filter for first-order traffic model in Lagrangian coordinates. In *Networking, Sensing and Control (ICNSC)*, 2011 IEEE International Conference on (pp. 121-126). IEEE.
- Zhang, H.M., 2002. A non-equilibrium traffic model devoid of gas-like behavior. *Transportation Research Part B* 36 (3), 275-290.